What causes the inverse relationship between primary production and export efficiency in the Southern Ocean?

Frédéric A. C. Le Moigne[1,2], Stephanie A. Henson[1], Emma Cavan[3], Clément Georges[4], Katsiaryna Pabortsava[3], Eric P. Achterberg[2,3], Elena Ceballos-Romero[5], Mike Zubkov[1], and Richard J. Sanders[1]

[1]National Oceanography Centre, Southampton, UK, [2]GEOMAR, Helmholtz Centre for Ocean Research Kiel, Kiel, Germany, [3]National Oceanography Centre, University of Southampton, Southampton, UK, [4]Laboratoire d'Océanologie et de Géosciences, Université du Littoral Côte d'Opale, ULCO, INSU-CNRS, UMR 8187 LOG, Wimereux, France, [5]Departamento de Física Aplicada II, Universidad de Sevilla, Sevilla, Spain

Abstract The ocean contributes to regulating atmospheric CO_2 levels, partly via variability in the fraction of primary production (PP) which is exported out of the surface layer (i.e., the *e* ratio). Southern Ocean studies have found that contrary to global-scale analyses, an inverse relationship exists between *e* ratio and PP. This relationship remains unexplained, with potential hypotheses being (i) large export of dissolved organic carbon (DOC) in high PP areas, (ii) strong surface microbial recycling in high PP regions, and/or (iii) grazing-mediated export that varies inversely with PP. We find that the export of DOC has a limited influence in setting the negative *e* ratio/PP relationship. However, we observed that at sites with low PP and high *e* ratios, zooplankton-mediated export is large and surface microbial abundance low suggesting that both are important drivers of the magnitude of the *e* ratio in the Southern Ocean.

1. Introduction

Over the last decades, algorithms have been developed to predict surface ocean carbon export, often based on satellite-derived estimates of primary production (PP) and sea surface temperature (SST). These algorithms are widely used and typically predict an increase in carbon flux with PP [*Dunne et al.*, 2007; *Laws*, 2011; *Laws et al.*, 2000]. Recently, however, an inverse relationship between surface ocean PP and export efficiency (*e* ratio, defined as the ratio between PP and particulate organic carbon (POC) flux exported from the upper ocean [*Buesseler*, 1998]) has been observed in the Southern Ocean (SO) [*Cavan et al.*, 2015; *Laurenceau-Cornec et al.*, 2015; *Maiti et al.*, 2013; *Morris et al.*, 2007; *Savoye et al.*, 2008]. A model study also found an inverse relationship between surface PP and *e* ratios for waters with SST < 7°C [*Henson et al.*, 2015] (their Figure 2a). This implies that existing empirical algorithms to predict carbon export may suffer from a significant bias in the SO. As the SO plays a crucial role in the global carbon cycle because of its unique features involving both biological processes and physical circulation [*Joos et al.*, 1991; *Pondaven et al.*, 2000; *Sarmiento and Orr*, 1991; *Sarmiento et al.*, 2004], resolving the cause of potential biases is key. The result is that the biological carbon pump may not be as efficient as previously assumed in low-temperature regions with enhanced productivity, as previously highlighted in *Lam and Bishop* [2007].

The processes driving the inverse relationship between PP and *e* ratio in the SO remain unclear, limiting our ability to develop improved export parameterizations. Zooplankton grazing, surface ocean bacterial recycling, and enhanced downward export flux of DOC are equally plausible drivers [*Cavan et al.*, 2015; *Hansell et al.*, 2009; *Laurenceau-Cornec et al.*, 2015; *Maiti et al.*, 2013].

Cavan et al. [2015] reported that variability in zooplankton abundance could explain up to 40% of the variance in the relationship between PP and *e* ratio in the SO. *Laurenceau-Cornec et al.* [2015] also investigated the impact of community structure on *e* ratios and found that variability in both phytoplankton and zooplankton abundance could explain the negative relationships. However, the contribution of both surface ocean bacterial particulate organic matter recycling and downward export of DOC to explain the trend in PP versus *e* ratio remains virtually unexplored.

The Scotia Sea in the Atlantic sector of the SO encompasses nearly all the different regimes the SO displays in terms of carbon export and PP: natural iron fertilization from the islands of South Georgia, high-nutrient,
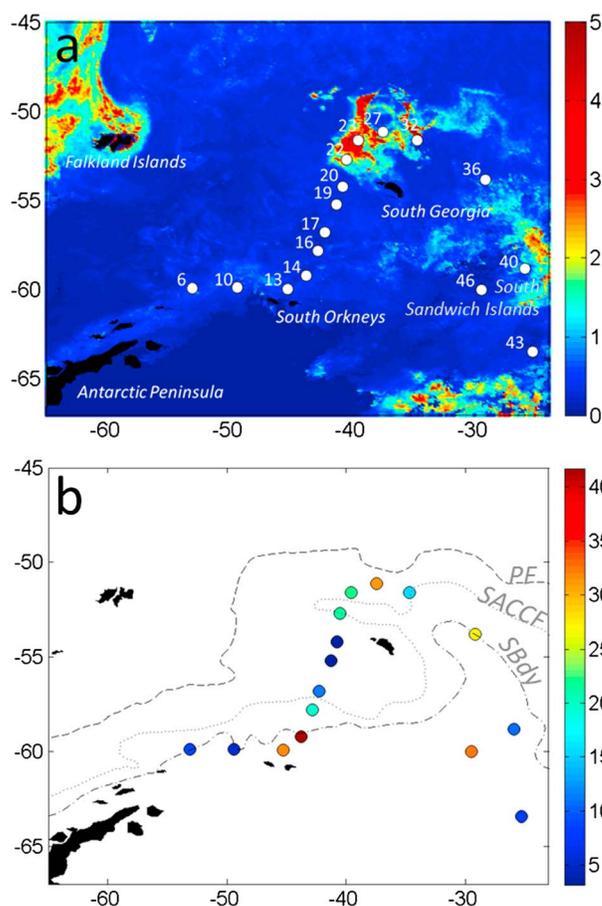
Figure 1. (a) Sampling stations and satellite-derived mean January–February 2013 (see section 2) chlorophyll *a* concentration ($\mu g\,L^{-1}$) and (b) POC export ($mmol\,m^{-2}\,d^{-1}$) in the Scotia Sea in January–February 2013. Front positions are indicated following *Orsi et al.* [1995]. PF stands for polar front, SACCF for Southern Antarctic Circumpolar Current Front, and SBdy for southern boundary of the Antarctic Circumpolar Current.

low-chlorophyll (HNLC) waters, and waters influenced by seasonal ice retreat [*Nielsdöttir et al.*, 2012]. The Scotia Sea is therefore a good natural laboratory to test the potential causes of the observed inverse relationship between PP and *e* ratio [*Cavan et al.*, 2015; *Maiti et al.*, 2013] over a larger spatial scale in the SO.

Here we further explore the processes that may explain the inverse relationship between PP and *e* ratio by comparing our estimates of *e* ratio with the zooplankton fecal pellet flux [*Cavan et al.*, 2015], the downward export of DOC, and surface-integrated bacterial and heterotrophic flagellate abundance, used as simple indicators of surface bacterial recycling rates.

2. Methods

Sampling took place from 11 January to 5 February 2013 on board RRS *James Clark Ross*, across the Scotia Sea (Figure 1) during cruise JR274. Discrete water samples were collected using a Rosette equipped with 24×20 L Ocean Test Equipment bottles and a conductivity-temperature-depth Seabird® sensor package including fluorescence.

2.1. POC Export Fluxes

Total ^{234}Th was precipitated from seawater samples using a small-volume technique (4 L) following *Pike et al.* [2005], with addition of a ^{230}Th spike. All the samples were purified and processed for ^{230}Th recovery analysis using a multicollector inductively coupled plasma–mass spectrometry (NEPTUNE Thermo Fisher) with addition of ^{229}Th as internal standard as described in *Pike et al.* [2005]. Recoveries yielded $90.0 \pm 3.6\%$ to calculate the ^{234}Th activity at the sampling time. Further information is provided in the supporting information Text S1 and Figures S1–S3. When looking at export efficiency, there is strong evidence showing that using the base of the euphotic zone (Ez) as export depth (i.e., integration depth for the ^{234}Th technique) is appropriate [*Buesseler and Boyd*, 2009]. However, in our study site, particle export likely occurred below the Ez depth as seen in the ^{234}Th:^{238}U ratio which is often <1 below the Ez depth (Figure S3). This was previously observed and discussed in *Rosengard et al.* [2015] in various sectors of the SO. For the sake of comparison, we decided to follow the approach of *Maiti et al.* [2013] and thus also use an export depth of 100 m to integrate our ^{234}Th activity. The choice of the export depth is further justified and discussed in detail in the supporting information Text S1 where we compare our *ThE_i* estimates following *Buesseler and Boyd* [2009] and *Maiti et al.* [2013] (and associated Figure S3 and Table S1 where Ez depth and mixed layer depths are provided). We calculated export rates of ^{234}Th based on a one-box model [*Buesseler et al.*, 1992] assuming steady state conditions and no supply of ^{234}Th related to physical processes. The data are described in full in *Le Moigne et al.* [2014]. Large (>53 μm) particles were collected by filtration of large volumes of seawater (1000–2500 L) through 53 μm mesh filters (293 mm diameter, NITEX®), using in situ pumps (Stand Alone Pumping Systems, Challenger Oceanic®) and analyzed for POC and particulate ^{234}Th as described in *Le Moigne et al.* [2013]. The pumps were deployed at 10 m below the mixed layer depth (defined as the depth at which the change from the surface temperature is 0.5°C). We did not

deploy pumps at the base of the euphotic zone because at several occasions the Ez depth was located above the mixed layer depth (Table S1 and Figure S3) which would have resulted in a large overestimation of the C:Th ratio and thus the POC flux because of the inclusion of nonsinking material [*Buesseler et al.*, 2006]. The choice of depth for the C:Th ratio and their variations are further discussed in the supporting information Text S1 (and associated Figures S2 and S3).

2.2. Primary Production

The Vertically Generalized Production Model (VGPM) estimates of satellite-derived PP [*Behrenfeld and Falkowski*, 1997] are freely available from (http://www.science.oregonstate.edu/ocean.productivity/). The VGPM is a commonly used algorithm for estimating regional or global ocean PP. PP was estimated in a box of size $0.5° \times 0.5°$ around each station (Figure 1) and integrated over 24 days, corresponding to the half-life of ^{234}Th. The E_i is then Th export/integrated PP, as in *Henson et al.* [2011].

2.3. Zooplankton Data

The marine snow catcher [*Riley et al.*, 2012] was used to quantify the flux of fecal pellets [*Cavan et al.*, 2015]. All zooplankton data are presented and described in *Cavan et al.* [2015].

2.4. Dissolved Organic Carbon Flux

Samples for DOC were filtered on precombusted (450°C, 4 h) Whatman GF/F filters into high-density polyethylene bottles cleaned with acid and frozen at −20°C for further analysis. DOC was analyzed using a Shimadzu TOC VCSH total organic carbon analyzer [*Pan et al.*, 2005]. Vertical diffusivity has, by definition, no direction. The direction of the flux is dictated by the gradient of the considered solute, here DOC. The DOC concentrations were higher in the surface (Figure S4), so the flux is downward. Downward fluxes of DOC were determined by multiplying the vertical gradient of DOC at 100 m (mol m^{-4}) by the averaged Scotia Sea vertical diffusivity (cm^2 s^{-1}). The vertical diffusivity was calculated following procedures presented and described in *Garabato et al.* [2004] and *Sheen et al.* [2013]. We averaged vertical diffusivity profiles (Kz $= 7.5 \times 10^{-3}$ cm^2 s^{-1}) measured in the Scotia Sea over a similar transect as ours [*Sheen et al.*, 2013]. Averaging presents a risk of overlooking spatial and temporal variability; however, in the surface, variability in vertical diffusivity is limited [*Sheen et al.*, 2013] (their Figures 4e–4h). Original diffusivity data are presented and discussed in *Sheen et al.* [2013].

2.5. Bacterioplankton and Protist Abundance

Abundance of bacteria and heterotrophic nanoflagellates from 0 to 300 m were measured using flow cytometry. The 1.6 mL of seawater was spiked with paraformaldehyde (PFA, 1% final concentration) just after sampling in 2 mL polypropylene vials. Samples were kept in a fridge (4°C) up to 12 h before analysis. SYBR Green I nucleic acid dye was used to stain the samples. Samples were then analyzed using a FACSort flow cytometer (BD, Oxford) calibrated with internal bead standards following procedures presented in *Zubkov and Burkill* [2006] and *Zubkov and Tarran* [2008].

3. Results and Discussion

3.1. Regional Description

The survey area (Figure 1) crossed two major SO fronts (see Figure 1), the Southern Boundary of the Antarctic Circumpolar Current (SBdy) and the South Antarctic Circumpolar Current Front (SACCF) as defined in *Orsi et al.* [1995]. All the sampled stations were located south of the polar front (PF). The satellite chlorophyll (Chl *a*) distribution for the survey area (Figure 1) and fluorescence profiles (Figure S3) showed a large bloom north of South Georgia Island (SGI) (stations 22, 23, and 27) and also near the South Sandwich Islands (SSI) (stations 36 and 40). Chl *a* concentrations were lowest in the Weddell Gyre (stations 43 and 46), in the central Scotia Sea (stations 14 and 16), and north of the South Orkney Islands (SOK).

3.2. Particulate Organic Carbon Fluxes and Primary Production

Vertical profiles of ^{234}Th:^{238}U activity ratios, POC:^{234}Th, and the integrated ^{234}Th fluxes (see section 2) are presented in Figure S3 and Table S1 and further discussed in the supporting information. The POC export fluxes (Figure 1 and Table S1) were highest north of the SOK, within the SGI bloom (stations 22–27) and near

the SSI (stations 36 and 46), as indicated by the ^{234}Th fluxes. The lowest fluxes were recorded south of the SGI bloom (stations 19 and 20, 3.2 ± 1.3 to $3.3 \pm 1.4 \, \mathrm{mmol\, m^{-2}\, d^{-1}}$) confirming suggestions made by *Korb et al.* [2012] about low POC export in the region. However, our results contrast with conclusions of *Korb et al.* [2012] who hypothesized that low POC fluxes also occur north of the SOK where we found our highest POC fluxes.

Integrated PP estimated following *Behrenfeld and Falkowski* [1997] displayed a similar geographical pattern to the satellite-derived Chl *a* described in section 3.1. Highest PP reached $129–259 \, \mathrm{mmol\, m^{-2}\, d^{-1}}$ in the SGI bloom (stations 22–32) while the lowest PP was recorded in the Weddell Gyre (stations 43 and 46) at $33–36 \, \mathrm{mmol\, m^{-2}\, d^{-1}}$. Elsewhere, PP was relatively homogenous with an average of $74 \pm 11 \, \mathrm{mmol\, m^{-2}\, d^{-1}}$ ($\pm$ standard deviation, $n = 11$).

3.3. Fecal Pellets, Dissolved Organic Carbon Fluxes, and Surface Microbial Abundance

Fecal pellet (FP) fluxes (POC flux associated with fecal pellets) during JR274 are presented and discussed in *Cavan et al.* [2015]. The FP flux was measured at fewer stations than the Th-derived POC export (Table S2). The FP flux ranged from 0 to $5.0 \, \mathrm{mmol\, m^{-2}\, d^{-1}}$ at stations 16 (stations 27 and 40) and 43, respectively. A high FP export ($3.5–5 \, \mathrm{mmol\, m^{-2}\, d^{-1}}$) was observed in the seasonal ice zone (stations 43–46) at 10 m below the mixed layer depth [*Cavan et al.*, 2015] even though total zooplankton abundance ($3–6 \times 10^3 \, \mathrm{ind.\, m^{-2}}$) was onefold lower in this region relative to the bloom region (stations 22–23) [*Cavan et al.*, 2015].

Vertical profiles of DOC are presented in Figure S4. DOC downward fluxes ranged from 0.27 to $0.41 \, \mathrm{mmol\, m^{-2}\, d^{-1}}$ (at Sts 46 and 16, respectively). No clear geographical pattern was evident in the spatial distribution of downward DOC export flux in the Scotia Sea (Table S2).

Vertical profiles of bacterial abundance and heterotrophic flagellates are presented in Figures S5 and S6, respectively. Largest integrated (top 100 m) abundances of bacteria were observed in the SGI bloom (stations 27–32), near the SSI (stations 32, 36, and 40), and the lowest in the Weddell Gyre (stations 43 and 46). Although the surface abundances of bacteria were not particularly large in the SGI bloom, the bacterial community contained a larger proportion of high nucleic acid (HNA) bacteria (Figure S4), reflecting higher activity [*Piontek et al.*, 2014], as HNA cells are normally responsible for the majority of the total bacterial production [*Lebaron et al.*, 2001]. Conversely, stations in the Drake Passage (stations 6 and 10) and the southernmost station (station 43) have the highest proportion of low nucleic acid containing bacteria (Figure S5). Surface-integrated abundance (top 100 m) of bacterioplankton and heterotrophic nanoflagellates are presented in Table S2.

3.4. Primary Production and *e* Ratio

The highest ThE_i ratios (>0.3) were observed north of the SOK (stations 13, 14, and 16), near the SSI (station 36), and at one station in the Weddell Gyre (station 46) (Table S2). Within the SGI bloom (stations 22–23), ThE_i were among the lowest recorded during the survey (0.06–0.08). Immediately south of the SGI bloom, stations 19 and 20 also displayed a low ThE_i. This further highlights the large variability of ThE_i even over a fairly limited space and time scale [*Henson et al.*, 2011; *Jacquet et al.*, 2011; *Le Moigne et al.*, 2015; *Planchon et al.*, 2015]. ThE_i ratio was poorly correlated with SST ($r^2 = 0.14$, $p = 0.147$, $n = 16$) as also reported by *Maiti et al.* [2013].

The relationship between the ThE_i ratio and PP obtained during summer 2013 in the Scotia Sea indicates a ThE_i ratio decrease with increasing PP (Figure 2c), consistent with recent observations [*Cavan et al.*, 2015; *Maiti et al.*, 2013]. This further challenges previous work which reported positive relationships between PP and ThE_i ratio (or *e* ratio) [*Laws*, 2011; *Laws et al.*, 2000] for a given temperature. Our relationship is

$$e - \mathrm{ratio} = -0.5381 (\pm 0.2149) \times \mathrm{Log(PP)} + 1.2962\ (\pm 0.4192)\quad r^2 = 0.306,\ p = 0.025,\ n = 16 \quad (1)$$

However, using similar bins (0–500, 500–1000, 1000–2000, 2000–3000, 3000–4000, $>4000 \, \mathrm{mg\, m^{-2}\, d^{-1}}$) to group our data as in *Maiti et al.* [2013], the correlation between PP and *e* ratio becomes stronger:

$$e\ \mathrm{ratio} = -0.4971 (\pm 0.1178) \times \mathrm{Log(PP)} + 1.273\ (\pm 0.249)\quad r^2 = 0.8525,\ p = 0.023,\ n = 5 \quad (2)$$

Using similar bins, [*Maiti et al.*, 2013] found

$$e\ \mathrm{ratio} = -0.3482 \times \mathrm{Log(PP)} + 1.2239\quad r^2 = 0.9717,\ n = 8 \quad (3)$$

When looking at relationships between the ThE_i ratio and PP (ours and those published earlier [*Cavan et al.*, 2015; *Maiti et al.*, 2013]), one could immediately suspect no independence of the variables because of
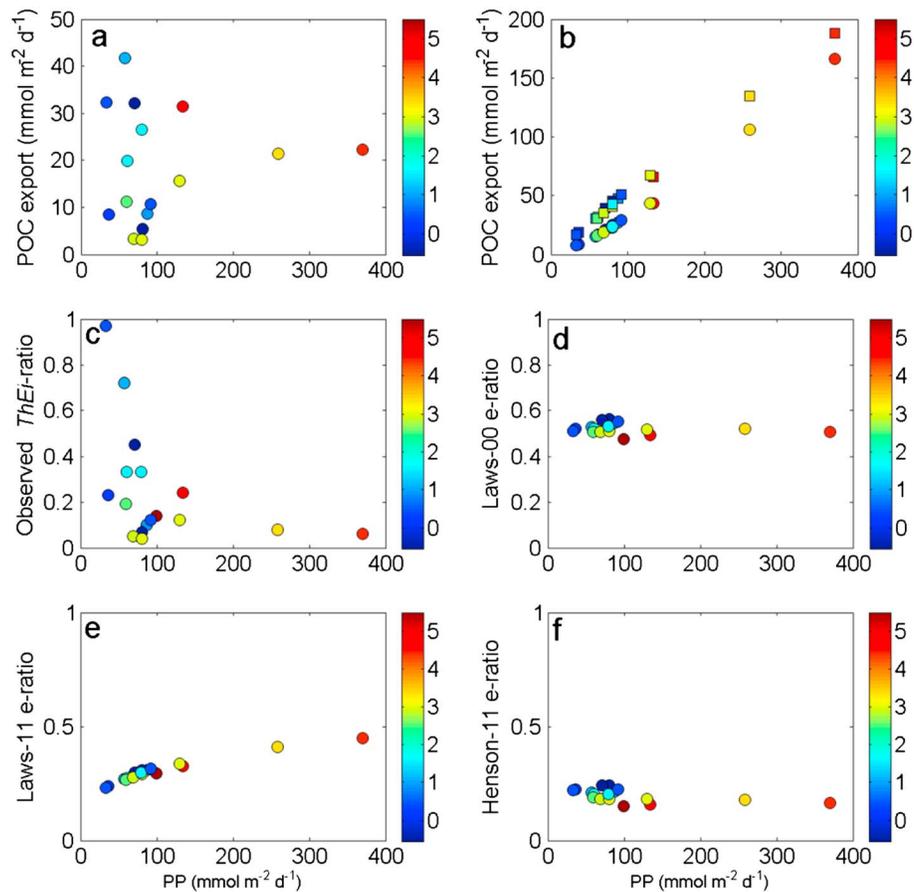
Figure 2. Scatterplot of POC export and primary production based on (a) our observations and (b) algorithms of *Laws et al.* [2000] (squares) and *Laws* [2011] (circles). Scatterplot of *e* ratio and primary production based on (c) observed *ThE_i* ratio and *e* ratio derived (d) from *Laws et al.* [2000] (Laws-00), (e) from *Laws* [2011] (Laws-11), and (f) from *Henson et al.* [2011] (Henson-11) algorithms. The color bar represents sea surface temperature (°C).

plotting POC export/PP versus PP. We do acknowledge that these relationships overlook some of the variability in both PP and POC export. However, in most of the global ocean, PP and export efficiency are positively correlated, in direct opposition to the inverse relationship in the SO first demonstrated by *Maiti et al.* [2013]. To demonstrate that this relationship is not simply an artifact of plotting POC export/PP versus PP, we plot POC export versus PP in Figure 2a. We see that at low PP stations ($<100 \, \text{mmol m}^{-2} \, \text{d}^{-1}$), POC export is variable but can be quite high, whereas at high PP station ($>100 \, \text{mmol m}^{-2} \, \text{d}^{-1}$), the POC export is relatively constant. Contrastingly, when plotting POC export calculated from PP and SST as in *Laws* [2011] and *Laws et al.* [2000] versus PP (Figure 2b), a clear positive correlation is observed in direct contrast to our observations.

Using existing SST- and PP-based algorithms [*Henson et al.*, 2011; *Laws*, 2011; *Laws et al.*, 2000] to predict *e* ratios, we find that they only capture a limited fraction of the observed range in *e* ratio (Figures 2d–2f). For instance, while our *ThE_i* ranges from 0.07 to 0.97 (Table S2), *e* ratio estimated using *Laws et al.* [2000] ranges from just 0.45 to 0.6 and from 0.1 and 0.3 using *Henson et al.* [2011]. A recent empirical algorithm [*Laws*, 2011] produces a larger range in *e* ratio (0.2 to 0.5, Figure 2e) but is still not consistent with the observed *ThE_i* ratios (observed and predicted *ThE_i* ratios are poorly correlated ($r^2 = 0.25$, $p = 0.0445$, $n = 16$)). Although the SST measured in the study region spans only a limited range (−0.5 to 4.8°C), none of the current algorithms (Figures 2d–2f) fully depicts the decreasing trend between *ThE_i* and PP we observed (Figure 2c). Indeed, *Laws* [2011] has the opposite trend to our observed pattern of low export efficiencies at high PP and high export efficiencies at low PP (Figure 2).

3.5. Drivers of High Productivity, Low Export (HPLE) Regimes

An inverse relationship between *e* ratio and PP (equations (1) and (2)) means that in high PP regions like the iron-fertilized areas of the SO, a large proportion of the PP is not readily exported as POC (low *e* ratio), while in
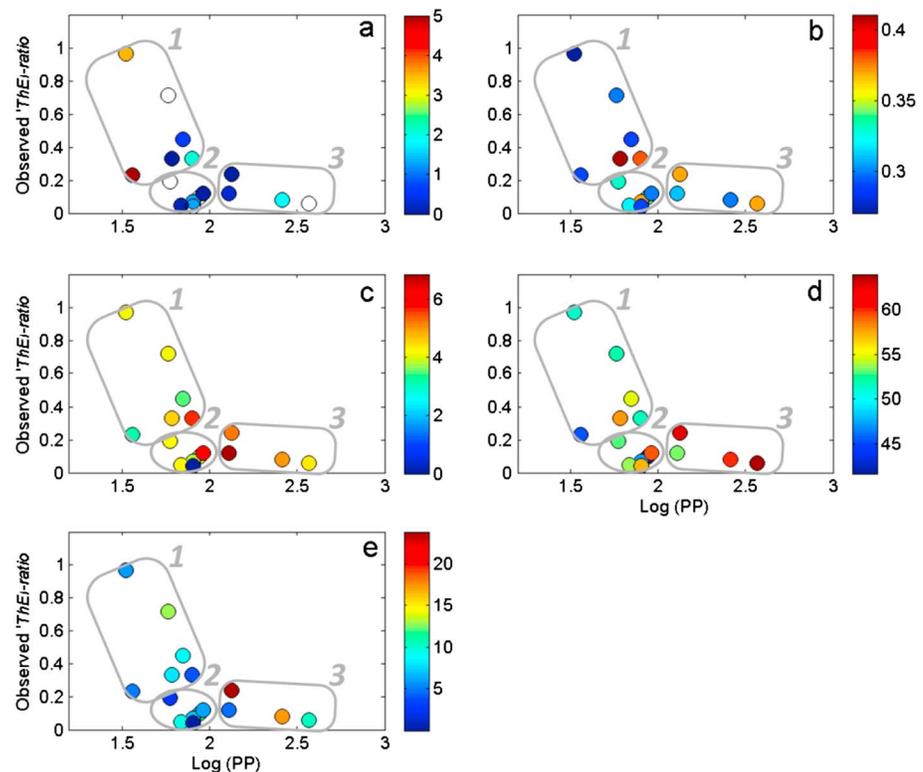
Figure 3. Observed ThE_i ratio versus log(PP). Color bars represent (a) flux of FP (mmol m^{-2} d^{-1}) from *Cavan et al.* [2015], (b) flux of DOC (mmol m^{-2} d^{-1}), (c) integrated bacterial abundance ($\times 10^{13}$ cell m^{-2}), (d) proportion of high nucleic acid containing bacteria over the total abundance of bacteria (%), and (e) integrated heterotrophic nanoflagellate abundance ($\times 10^{10}$ cell m^{-2}). We diagnosed three distinct groups of stations based on their ThE_i ratio (below or above 0.2) and their PP (below or above 100 mmol m^{-2} d^{-1}): (1) a low PP, high ThE_i ratio group (stations 13, 14, 16, 36, 43, and 46), (2) a low PP, low ThE_i ratio group (stations 6, 10, 17, 19, 20, and 40), and (3) a high PP, low ThE_i ratio group (stations 22, 23, 27, and 32).

regions where the PP is low (such as the HNLC regions), a large proportion of the PP can be exported as POC. Potentially, this can be attributed to temporal decoupling between PP and subsequent export [*Henson et al.*, 2015] and by extension to the time scales over which PP and export are integrated. For instance, *Maiti et al.* [2013] calculated their *e* ratio using Th-derived POC export and ^{14}C in situ measurements of PP, which integrate PP and POC export over different time scales despite being sampled at the same time (^{14}C PP is instantaneous, and Th export time scale is ~1 month [*Le Moigne et al.*, 2013]). *Cavan et al.* [2015], *Laurenceau-Cornec et al.* [2015], and *Maiti et al.* [2013] also coupled ^{14}C in situ measurements of PP and more instantaneous measurements of POC export using the marine snow catcher [*Riley et al.*, 2012], surface-tethered particle interceptor sediment traps [*Knauer et al.*, 1979], or traditional traps. Despite the potential for issues associated with PP and export temporal decoupling as described in *Henson et al.* [2015], they all observe inverse relationships between *e* ratio and PP. Here we used the ThE_i ratio, which integrates PP and export over similar time scales (see explanation of integration time in *Henson et al.* [2011]). This should minimize issues related to temporal decoupling; however, we cannot fully reject its influence, as the degree of seasonal variability at the study site and bloom phase also plays a role [*Henson et al.*, 2015]. Nevertheless, it seems likely that inverse relationships between *e* ratio and PP also result from ecosystem-related processes, not solely from mismatched integration time scales of the techniques used.

Cavan et al. [2015] and *Laurenceau-Cornec et al.* [2015] recently found that zooplankton grazing influences the relationship between *e* ratio and PP but does not fully explain it. We therefore hypothesize that the relationship may also additionally result from large DOC flux and/or vigorous surface bacterial recycling.

We now test these hypotheses by individually comparing the estimated fluxes of DOC and FP and the bacterioplankton and heterotrophic flagellate integrated abundance (Table S1 and Figures 3 and 4). We diagnosed three distinct groups of stations based on their ThE_i ratio (below or above 0.2) and their PP (below or above
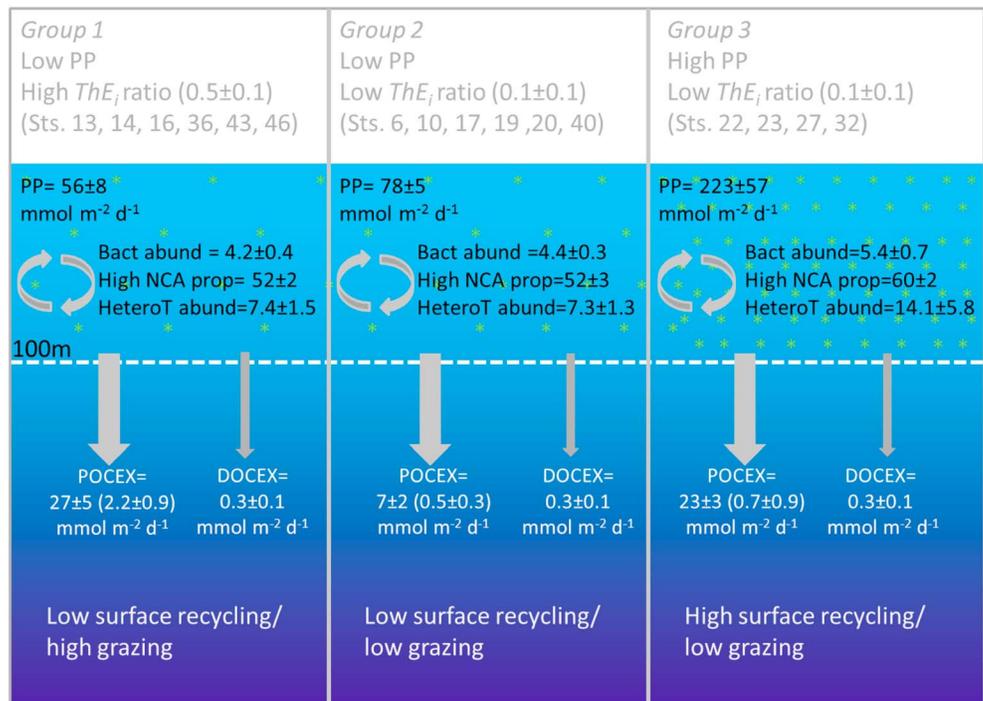
Figure 4. Schematic diagram of the primary production, carbon fluxes, and surface recycling indicators during JR274. POC fluxes presented in brackets are the fecal pellet flux published in *Cavan et al.* [2015]. Ranges are expressed as standard error of the mean.

100 mmol m^{-2} d^{-1}): (1) a low PP, high ThE_i ratio group (stations 13, 14, 16, 36, 43, and 46); (2) a low PP, low ThE_i ratio group (stations 6, 10, 17, 19, 20, and 40); and (3) a high PP, low ThE_i ratio group (stations 22, 23, 27, and 32) (Figures 3 and 4). If the DOC downward flux contributes to the inverse relationship (equation (2)), the DOC flux should be small in group 1 and large in group 3. This is because a large proportion of surface PP would exit the surface as DOC and not POC, thus lowering the ThE_i ratio. The downward flux of DOC was 0.3 ± 0.1, 0.3 ± 0.0, and 0.3 ± 0.1 mmol m^{-2} d^{-1} in groups 1, 2, and 3, respectively (Table S4 and Figures 3 and 4b). The flux of DOC is identical in all three groups and is small relative to the magnitude of the POC export flux (1–10% of the POC flux, Tables S1 and S2). At least for our Scotia Sea data set, DOC downward flux can therefore be ruled out as a factor driving the inverse relationship between PP and e ratio. On the seasonal scale, this may be different as DOC can also be exported as part of the restratification process in spring [*Xi et al.*, 2014]. This could potentially result in larger downward DOC flux than the downward diffusive flux presented here. Also, the flux of DOC is, by definition, not included in the ThE_i (or any export efficiency estimate apart from the f ratio [*Dugdale and Goering*, 1967] based ones) because ThE_i is the ratio of POC exported over PP. Although DOC flux is here negligible, at the global scale DOC is thought to contribute an extra ~20% to total export flux [*Hansell and Carlson*, 1998].

Alternatively, should the FP flux be responsible for this negative trend (Figure 2a), the FP flux should be small in groups 2 and 3 and large in group 1. An efficient packaging of senescent phytoplankton cells (potentially sinking slowly) into FP (likely fast sinking) could lead to a large proportion of the PP being exported as POC and thus high ThE_i ratio. This is consistent with the suggestion that in high PP regimes, the intensity of the phytoplankton bloom can on occasions be overwhelming for the zooplankton community resulting in the loss of the packaging function [*Lam et al.*, 2011]. The flux of FP in the study regions showed large variability [*Cavan et al.*, 2015]. However, the flux of FP (Figure 3a and Table S2) is indeed lower in groups 2 and 3 (0.5 ± 0.3 and 0.7 ± 0.9 mmol m^{-2} d^{-1}, respectively) than in group 1 (2.2 ± 0.9 mmol m^{-2} d^{-1}, Figure 4). The highest FP fluxes (3.5–5.0 mmol m^{-2} d^{-1}) also correspond to fairly high ThE_i ratios (0.23–0.97, Sts. 43 and 46) recorded during our survey. This suggests that FP flux and the type of FP (compact versus loose) are some of the factors driving the negative relationship between the ThE_i ratio and PP. It is possible that in high PP regions (group 3), the zooplankton community is not able to keep pace with the increasing phytoplankton biomass which accumulates in surface waters rather than being exported.

This is rather counterintuitive as phytoplankton cells can aggregate and sink. The lack of mineral ballast observed in the SO [*Le Moigne et al.*, 2014, 2012] could be a possible explanation for this. Nonmineralizing phytoplankton species such as *Phaeocystis sp.* have been observed in the iron-induced bloom around the Crozet Islands in the SO [*Poulton et al.*, 2007] and had a limited contribution to POC export [*Salter et al.*, 2007]. The ecological reason the FP is low in group 2 is unclear but may be related to the influence of ice retreat on the life cycles of zooplankton as suggested by *Cavan et al.* [2015].

Finally, we test the influence of surface-integrated bacterial abundance, their proportion of high nucleic acid cells (reflecting the proportion of actively growing versus dormant bacteria cells, a high nucleic acid community being more active [*Piontek et al.*, 2014]), and heterotrophic flagellate abundance, used as simple indicators of surface microbial recycling rates in the absence of measured bacterial production estimates. If bacterial activity is an important factor driving the relationship between the ThE_i ratio and PP, limited surface ocean recycling of particulate organic matter is expected in groups 1 and 2 with high recycling occurring in group 3. Stations belonging to group 3 show the highest integrated bacterial abundance ($5.4 \pm 0.7 \times 10^{13}$ cell $^{-2}$), high nucleic acid proportion ($60 \pm 2\%$, Figures 3c, 3d, and S5) and heterotrophic nanoflagellates ($14.1 \pm 5.8 \times 10^{10}$ cell m^{-2}, Figures 3e, 4, and S6). Conversely, in groups 1 and 2, the three indicators are substantially lower (Figures 3c–3e and 4). This suggests that surface recycling has a large influence in setting the inverse relationship between *e* ratio and PP in the SO. The reason station 43 displayed the highest FP flux (5.0 mmol m^{-2} d^{-1}) but a lower ThE_i ratio (0.23) than the nearby station 46 remains unclear given that both bacterial/ heterotrophic nanoflagellate abundance and the proportion of high nucleic acid bacteria over the total abundance of bacteria (Figure S5) were also lower.

Admittedly, our analysis suffers from the shortcoming that none of the processes tested (DOC and FP flux and surface microbial recycling indicators) are time integrated as is the ThE_i ratio. Therefore, we cannot exclude the possibility that the trends would either collapse or strengthen if the three indicators were adequately time integrated. Assessing this would only be possible with time-sustained observations of plankton and microbial community structure and associated biological rates. Nonetheless, our data strongly suggest that the DOC export has a limited influence in setting the inverse relationship between ThE_i ratio and PP in the Scotia Sea. Instead, as observed before [*Cavan et al.*, 2015; *Laurenceau-Cornec et al.*, 2015], the zooplankton community, through grazing and production/export of fecal pellets, appears to be an important factor. Moreover, we clearly show, for the first time, that surface ocean microbial recycling of particulate organic matter is critical in setting the ThE_i ratio as hypothesized by *Maiti et al.* [2013].

3.6. Implications for Export Algorithms

Our results have implications for our understanding of SO biogeochemistry and the algorithms used to predict POC export in this region. According to *Laws et al.* [2000], the *e* ratio is temperature dependent. They found that at low temperature, where the bacterial activity is expected to be low, the *e* ratio is high. However, and consistent with our findings, *Maiti et al.* [2013] showed no significant correlation between temperature and *e* ratio in cold waters (below 6°C). It is somehow paradoxical to find that a process like the export efficiency is on one hand partly driven by the magnitude of surface ocean bacterial recycling of particulate organic matter (temperature dependent) but on the other hand poorly correlated with water temperature. It is possible that the quality of the organic matter microbes are feeding on has an equally important role relative to temperature in regulating the surface microbial cycling and the zooplankton grazing and by extension the *e* ratio in the Scotia Sea.

Siegel et al. [2014] recently developed a new algorithm for POC export that, unlike previous empirical algorithms [*Henson et al.*, 2011; *Laws et al.*, 2000], provides a mechanistic representation of export. We plotted a prediction of the *e* ratio versus PP using the *Siegel et al.* [2014] algorithm (Figure S7). The *Siegel et al.* [2014] algorithm suggests a positive relationship between *e* ratio and PP (similar to *Laws et al.* [2000]), although not statistically significant at the 95% level (Figure S7), in contrast to our observed trend (Figure 2a). This either means that (1) the *Siegel et al.* [2014] mechanistic algorithm misses some fundamental processes driving the magnitude of the *e* ratio or (2) the *e* ratio is driven in a fundamentally different way in the SO than the rest of the global ocean (e.g., specific processes could be an important pathway for export in SO but insignificant elsewhere). Either way, it suggests that a global algorithm for POC export may be an unrealistic prospect. Consequently, the application of region-specific food web models for satellite-derived estimates of export seems necessary to fully represent the large global range in *e* ratio. It now seems clear that HPLE

regions are widespread in the SO [*Cavan et al.*, 2015; *Lam and Bishop*, 2007; *Laurenceau-Cornec et al.*, 2015; *Maiti et al.*, 2013]. In our data, the downward export of DOC had a limited impact on the magnitude of the ThE_i ratio, inconsistent with *Hansell et al.* [2009]. We believe that this is due to combined high surface bacterial activity and low grazing/fecal pellet export (Figures 3 and 4) in the high PP regions. We recommend that these two processes must be carefully taken into account in attempts to predict SO *e* ratio from PP estimates.

References

Behrenfeld, M. J., and P. G. Falkowski (1997), Photosynthetic rates derived from satellite-based chlorophyll concentration, *Limnol. Oceanogr.*, 42(1), 1–20.

Buesseler, K. O. (1998), The decoupling of production and particulate export in the surface ocean, *Global Biogeochem. Cycles*, 12(2), 297–310, doi:10.1029/97GB03366.

Buesseler, K. O., and P. W. Boyd (2009), Shedding light on processes that control particle export and flux attenuation in the twilight zone of the open ocean, *Limnol. Oceanogr.*, 54(4), 1210–1232.

Buesseler, K. O., M. P. Bacon, J. K. Cochran, and H. D. Livingston (1992), Carbon and nitrogen export during the JGOFS North Atlantic Bloom Experiment estimated from ^{234}Th:^{238}U disequilibria, *Deep-Sea Res. I*, 39(7–8), 1115–1137.

Buesseler, K. O., et al. (2006), An assessment of particulate organic carbon to thorium-234 ratios in the ocean and their impact on the application of ^{234}Th as a POC flux proxy, *Mar. Chem.*, 100(3–4), 213–233.

Cavan, E., F. A. C. Le Moigne, A. J. Poulton, C. J. Daniels, G. Fragoso, and R. J. Sanders (2015), Zooplankton fecal pellets control the attenuation of particulate organic carbon flux in the Scotia Sea, Southern Ocean, *Geophys. Res. Lett.*, 41, doi:10.1002/2014GL062744.

Dugdale, R. C., and J. J. Goering (1967), Uptake of new and regenerated forms of nitrogen in primary productivity, *Limnol. Oceanogr.*, 12(2), 196–206.

Dunne, J. P., J. L. Sarmiento, and A. Gnanadesikan (2007), A synthesis of global particle export from the surface ocean and cycling through the ocean interior and on the seafloor, *Global Biogeochem. Cycles*, 21(4), doi:10.1029/2006GB002907.

Garabato, A. C. N., K. L. Polzin, B. A. King, K. J. Heywood, and M. Visbeck (2004), Widespread intense turbulent mixing in the Southern Ocean, *Science*, 303(5655), 210–213.

Hansell, D. A., and C. A. Carlson (1998), Net community production of dissolved organic carbon, *Global Biogeochem. Cycles*, 12(3), 443–453, doi:10.1029/98GB01928.

Hansell, D. A., C. A. Carlson, D. J. Repeta, and R. Schlitzer (2009), Dissolved organic matter in the ocean: A controversy stimulates new insights, *Oceanography*, 22(4), 202–211.

Henson, S. A., A. Yool, and R. J. Sanders (2015), Variability in efficiency of particulate organic carbon export: A model study, *Global Biogeochem. Cycles*, doi:10.1002/2014GB004965.

Henson, S., R. Sanders, E. Madsen, P. Morris, F. A. C. Le Moigne, and G. Quartly (2011), A reduced estimate of the strength of the ocean's bioloical carbon pump, *Geophys. Res. Lett.*, 38, doi:10.1029/2011GL046735.

Jacquet, S. H. M., P. J. Lam, T. Trull, and F. Dehairs (2011), Carbon export production in the subantarctic zone and polar front zone south of Tasmania, *Deep Sea Res II*, 58, 2277–2292.

Joos, F., J. L. Sarmiento, and U. Siegenthaler (1991), Estimates of the effect of Southern Ocean iron fertilization on atmospheric CO_2 concentrations, *Nature*, 349(6312), 772–775.

Knauer, G. A., J. H. Martin, and K. W. Bruland (1979), Fluxes of particulate carbon, nitrogen, and phosphorus in the upper water column of the northeast Pacific, *Deep-Sea Res.*, 26(1), 97–108.

Korb, R., M. J. Whitehouse, P. Ward, M. Gordon, H. J. Venables, and A. J. Poulton (2012), Regional and seasonal differences in microplankton biomass, productivity, and structure across the Scotia Sea: Implications for export of biogenic carbon, *Deep Sea Res II*, 59–60, 67–78.

Lam, P. J., and J. K. B. Bishop (2007), High biomass, low export regimes in the Southern Ocean, *Deep-Sea Res II*, 54(5–7), 601–638.

Lam, P. J., S. C. Doney, and J. K. B. Bishop (2011), The dynamic ocean biological pump: Insights from a global compilation of particulate organic carbon, $CaCO_3$, and opal concentration profiles from the mesopelagic, *Global Biogeochem. Cycles*, doi:10.1029/2010GB003868.

Laurenceau-Cornec, E. C., et al. (2015), The relative importance of phytoplankton aggregates and zooplankton fecal pellets to carbon export: Insights from free-drifting sediment trap deployments in naturally iron-fertilised waters near the Kerguelen Plateau, *Biogeosciences*, 12, 1007–1027.

Laws, E. A. (2011), Simple equations to estimate ratios of new or export production to total production from satellite-derived estimates of sea surface temperature and primary production, *Limnol. Oceanogr. Methods*, 9, 593–601.

Laws, E. A., P. G. Falkowski, W. O. Smith, H. Ducklow, and J. J. McCarthy (2000), Temperature effects on export production in the open ocean, *Global Biogeochem. Cycles*, 14(4), 1231–1246, doi:10.1029/1999GB001229.

Le Moigne, F. A. C., R. J. Sanders, M. Villa-Alfageme, A. P. Martin, K. Pabortsava, H. Planquette, P. J. Morris, and S. J. Thomalla (2012), On the proportion of ballast versus non-ballast associated carbon export in the surface ocean, *Geophys. Res. Lett.*, 39, L15610, doi:10.1029/2012GL052980.

Le Moigne, F. A. C., M. Villa-Alfageme, R. J. Sanders, C. M. Marsay, S. Henson, and R. Garcia-Tenorio (2013), Export of organic carbon and biominerals derived from ^{234}Th and ^{210}Po at the Porcupine Abyssal Plain, *Deep Sea Res Part I*, 72, 88–101, doi:10.1016/j.dsr.2012.10.010.

Le Moigne, F. A. C., K. Pabortsava, C. L. J. Marcinko, P. Martin, and R. J. Sanders (2014), Where is mineral ballast important for surface export of particulate organic carbon in the ocean?, *Geophys. Res. Lett.*, 41, doi:10.1002/2014GL061678.

Le Moigne, F. A. C., A. J. Poulton, S. A. Henson, C. Daniels, G. Fragoso, et al. (2015), Carbon export efficiency and phytoplankton community composition in the Atlantic sector of the Arctic Ocean, *J Geophys Res Oceans*, 120, doi:10.1002/2015JC010700.

Lebaron, P., P. Servais, H. Agogue, C. Courties, and F. Joux (2001), Does the high nucleic acid content of individual bacterial cells allow us to discriminate between active cells and inactive cells in aquatic systems, *Appl. Environ. Microbiol.*, 67(4), 1775–1782.

Maiti, K., M. Charette, K. Buesseler, and M. Kahru (2013), An inverse relationship between production and export efficiency in the Southern Ocean, *Geophys. Res. Lett.*, 40, 1557–1561, doi:10.1002/grl.50219.

Morris, P. J., R. Sanders, R. Turnewitsch, and S. Thomalla (2007), ^{234}Th-derived particulate organic carbon export from an island-induced phytoplankton bloom in the Southern Ocean, *Deep Sea Res Part II*, 54(18–20), 2208–2232, doi:10.1016/j.dsr2.2007.06.002.

Nielsdóttir, M. C., T. S. Bibby, C. M. Moore, D. J. Hinz, R. J. Sanders, R. Korb, M. Whitehouse, and E. P. Achterberg (2012), Seasonal and continuous iron supply in the Scotia Sea, *Mar. Chem.*, 131–132, 62–72.

Orsi, A. H., T. Whitworth, and W. D. Nowlin (1995), On the meridional extent and fronts of the Antarctic Circumpolar Current, *Deep Sea Res Part I*, *42*(5), 641–673.

Pan, X., R. Sanders, A. D. Tappin, P. J. Worsfold, and E. Achterberg (2005), Simultaneous determination of Dissolved Organic Carbon and Total Dissolved Nitrogen on a Coupled High-Temperature Combustion Total Organic Carbon-Nitrogen Chemiluminescence Detection (HTC TOC-NCD) system, *J. Autom. Methods Manag. Chem.*, *4*, 240–246.

Pike, S. M., K. O. Buesseler, J. Andrews, and N. Savoye (2005), Quantification of ^{234}Th recovery in small volume sea water samples by inductively coupled plasma-mass spectrometry, *J. Radioanal. Nucl. Chem.*, *263*(2), 355–360, doi:10.1007/s10967-005-0062-9.

Piontek, J., M. Sperling, E. M. Nothig, and A. Engel (2014), Regulation of bacterioplankton activity in Fram Strait (Arctic Ocean) during early summer: The role of organic matter supply and temperature, *J. Mar. Syst.*, *132*, 83–94.

Planchon, F., D. Ballas, A. J. Cavagna, A. R. Bowie, D. Davies, T. Trull, E. C. Laurenceau-Cornec, P. van der Merwe, and F. Dehairs (2015), Carbon export in the naturally iron-fertilized Kerguelen area of the Southern Ocean based on the ^{234}Th approach, *Biogeosciences*, *12*, 38–3848, doi:10.5194/bg-12-3831-2015.

Pondaven, P., O. Ragueneau, P. Treguer, A. Hauvespre, L. Dezileau, and J. L. Reyss (2000), Resolving the "opal paradox" in the Southern Ocean, *Nature*, *405*(6783), 168–172.

Poulton, A. J., C. M. Moore, S. Seeyave, M. I. Lucas, S. Fielding, and P. Ward (2007), Phytoplankton community composition around the Crozet Plateau, with emphasis on diatoms and Phaeocystis, *Deep Sea Res Part II*, *54*, 2085–2105.

Riley, J., R. Sanders, C. Marsay, F. A. C. Le Moigne, E. Achterberg, and A. Poulton (2012), The relative contribution of fast and slow sinking particles to ocean carbon export, *Global Biogeochem. Cycles*, *26*, doi:10.1029/2011GB004085.

Rosengard, S. Z., P. J. Lam, W. M. Balch, M. E. Auro, S. Pike, D. Drapeau, and B. Bowler (2015), Carbon export and transfer to depth across the Southern Ocean Great Calcite Belt, *Biogeosciences*, *12*, 3953–3971.

Salter, I., R. S. Lampitt, R. Sanders, A. Poulton, A. E. S. Kemp, B. Boorman, K. Saw, and R. Pearce (2007), Estimating carbon, silica and diatom export from a naturally fertilised phytoplankton bloom in the Southern Ocean using PELAGRA: A novel drifting sediment trap, *Deep Sea Res Part II*, *54*(18–20), 2233–2259, doi:10.1016/j.dsr2.2007.06.008.

Sarmiento, J. L., and J. C. Orr (1991), 3-dimensional simulations of the impact of Southern Ocean nutrient depletion on atmospheric CO_2 and ocean chemistry, *Limnol. Oceanogr.*, *36*(8), 1928–1950.

Sarmiento, J. L., N. Gruber, M. A. Brzezinski, and J. P. Dunne (2004), High-latitude controls of thermocline nutrients and low latitude biological productivity, *Nature*, *427*(6969), 56–60, doi:10.1038/nature02127.

Savoye, N., T. W. Trull, S. H. M. Jacquet, J. Navez, and F. Dehairs (2008), ^{234}Th-based export fluxes during a natural iron fertilization experiment in the Southern Ocean (KEOPS), *Deep Sea Res Part II*, *55*, 841–855.

Sheen, K. L., J. A. Brearley, A. C. Naveira Garabato, D. A. Smeed, S. Waterman, et al. (2013), Rates and mechanisms of turbulent dissipation and mixing in the Southern Ocean: Results from the Diapycnal and Isopycnal Mixing Experiment in the Southern Ocean (DIMES), *J. Geophys. Res. Oceans*, *188*, 2774–27,952, doi:10.1002/jgrc.20217.

Siegel, D. A., K. O. Buesseler, S. C. Doney, S. F. Sailley, M. J. Behrenfeld, and P. W. Boyd (2014), Global assessment of ocean carbon export by combining satellite observations and food-web models, *Global Biogeochem. Cycles*, *28*, 181–196, doi:10.1002/2013GB004743.

Xi, P., E. P. Achterberg, R. J. Sanders, A. J. Poulton, K. I. Oliver, and C. Robinson (2014), Dissolved organic carbon and apparent oxygen utilization in the Atlantic Ocean, *Deep Sea Res Part I*, *85*, 80–87.

Zubkov, M. V., and G. A. Tarran (2008), High bacterivory by the smallest phytoplankton in the North Atlantic Ocean, *Nature*, *455*, doi:10.1038/nature07236).

Zubkov, M. V., and P. H. Burkill (2006), Syringe pumped high speed flow cytometry of oceanic phytoplankton, *Cytometry A*, *69*, 1010–1019.